Journal of Solid State Chemistry 181 (2008) 1670–1677

Contents lists available at ScienceDirect

Journal of Solid State Chemistry

journal homepage: www.elsevier.com/locate/jssc

Electrostatic characteristics of nanostructures investigated using electric force microscopy

X.H. Qiu *, G.C. Qi, Y.L. Yang, C. Wang *

National Center for Nanoscience and Technology, Beijing 100080, PR China

ARTICLE INFO

Article history:
Received 10 April 2008
Received in revised form
17 June 2008
Accepted 18 June 2008
Available online 20 June 2008

Keywords:
Electric force microscopy
Electrostatic characteristics
Nanostructures
Nanomaterials

ABSTRACT

Nanosized materials possess many interesting physical and chemical properties that differ significantly from their macroscopic counterparts. Understanding the size- and shape-dependent properties of nanostructures are of great value to rational design of nanomaterials with desired functionality. Electric force microscopy (EFM) and its variations offer unique opportunities to deepen our insights into the electrical characteristics of nanostructures. In this paper, we review recent progress of this versatile technique and its applications in studying the electrical properties of nanosized materials. A variety of important issues in EFM experimentation and theoretical modeling are discussed, with an emphasis on the ongoing efforts to improve the precision in quantitative measurements of charge density and dielectric properties of nanostructures.

© 2008 Elsevier Inc. All rights reserved.

1. Introduction

Nanostructured materials are a new class of materials whose unique physical and chemical properties offer great potentials for applications in bio-imaging, sensing, and miniaturized electronic devices. With recent progress in controlled synthesis of nanomaterials, research interests in the field have been more focused on developing a comprehensive understanding of the structure–property correlations of these novel materials. In this respect, the advancement of characterization methods capable of directly yielding structural information and measuring various properties at the nanometer scale would provide the infrastructural support to the emerging nanotechnology.

Electrical characteristics of nanosized structures is one of the important aspects of their physical and chemical properties. Due to quantum confinement effect, the electrical properties of nanostructures depend sensitively on their geometrical dimensions [1]. The application of electric force microscopy (EFM) on studying nanocrystals and nanowires has enriched the understanding of charge distribution, dielectric behavior of the nanostructures and generated extensive interests in exploring the functionalities of these nanomaterials.

EFM is essentially an atomic force microscope (AFM) with a conductive probe electrically biased with respect to the sample. When lifted over the sample surface, the probe interacts with the sample through long-range Coulomb forces. By this means, spatial variations in surface charge or local work function of sample would change the amplitude and phase for an oscillating cantilever, generating a contrast in the electrostatic force experienced by the probe. The methodology of employing a scanning proximal probe enables simultaneous mapping of surface topography and corresponding electrostatic properties of samples with lateral resolution down to the nanometer scale, making EFM a versatile technique for studying charge density and dopant distribution [2–4], profiling electric field and potential in devices [5–7], identifying ferroelectric phase transition in nanocrystals [8], and measuring dielectric properties of nanostructures [9,10]. Depending on the method and recorded signal in measurement, electrostatic force techniques are known by a variety of names, including the generic EFM, scanning capacitance microscopy (SCM), Kelvin probe microscopy (KPM), scanning polarization force microscopy (SPFM), and possibly others.

EFM made its debut as a non-destructive technique for device characterization, such as detecting the dielectric coating on Si wafer and performing potentiometric measurements over the passivated p–n junction in a commercial transistor [11]. Electric force as small as 10^{-10} N, corresponding to a capacitance of 10^{-19} F, was measured experimentally by applying a modulating voltage to an oscillating AFM tip. The scheme improves the detection resolution of capacitance compared with previously reported scanning capacitance microscope [12] and provides independent measures of capacitance and topography simultaneously. At the mean time, a force microscope based on similar principle was proposed and applied to study the metal–insulator

* Corresponding authors.
E-mail addresses: xhqiu@nanoctr.cn (X.H. Qiu), wangch@nanoctr.cn (C. Wang).

0022-4596/$ - see front matter © 2008 Elsevier Inc. All rights reserved.
doi:10.1016/j.jssc.2008.06.036

contact electrification [13]. Bipolar charging was achieved by bringing a biased tip in contact with sample surface. Charge features as small as 0.2 μm were identified in the charge images [13]. In addition to imaging the localized surface charges, EFM was also used to investigate the migration of surface ions driven by the fringe electric field in the vicinity of an open-gate field-effect transistor, yielding useful information for device designers to reduce device instabilities [14].

The dual functions of EFM to manipulate and detect the charge state on the nanometer scale provide a powerful method for gaining insight into the electrostatic characteristics of nanostructures. Using EFM tip as a localized electron source, charge injection kinetics in nanoparticles supported on conductive substrate with thin silicon oxide film was investigated [15,16]. It was found that electrons could successively tunnel through the tip–nanoparticle–substrate double junctions and generate an equilibrium charge state on the nanoparticles [16]. The charges stored in the nanoparticles as a function of charging voltage was studied and calculated quantitatively by using an analytical model which determines the amount of charges by the ratio between the static-charge versus capacitive force gradients [15,17,18]. Besides the contribution from capacitive and static-charge interactions, a much weaker dipole–dipole interactions originated from surface dipole was identified in the EFM force spectroscopy [17].

Charge injection and transport in single-walled carbon nanotubes (SWCNTs) and multiwalled carbon nanotubes (MWCNTs) deposited on insulator surface have been systematically studied using EFM [19–21]. All of the nanotubes in studies behaved as good electron reservoir and possessed good charging and discharging properties. The delocalized charges in carbon nanotubes (CNTs) preferably discharged when EFM tips came close to the ends of CNTs, indicating a locally enhanced electric field around CNTs caps. Even after discharging, the enhanced emission pattern was still evident in the halo formed by residual charges in the oxide adjacent to CNTs [19,20].

At low temperature, EFM is sensitive enough to detect single-electron charging events in confined systems such as individual semiconductor quantum dots [22] and carbon nanotubes segmented by local defects [23]. The Coulomb blockade effect exhibited as a series of discontinuous steps observed in the dynamical response of EFM cantilever. When electrons moved on/off each segments of carbon nanotube, concentric patterns of Coulomb oscillations were seen in EFM images as shown in Fig. 1 [23].

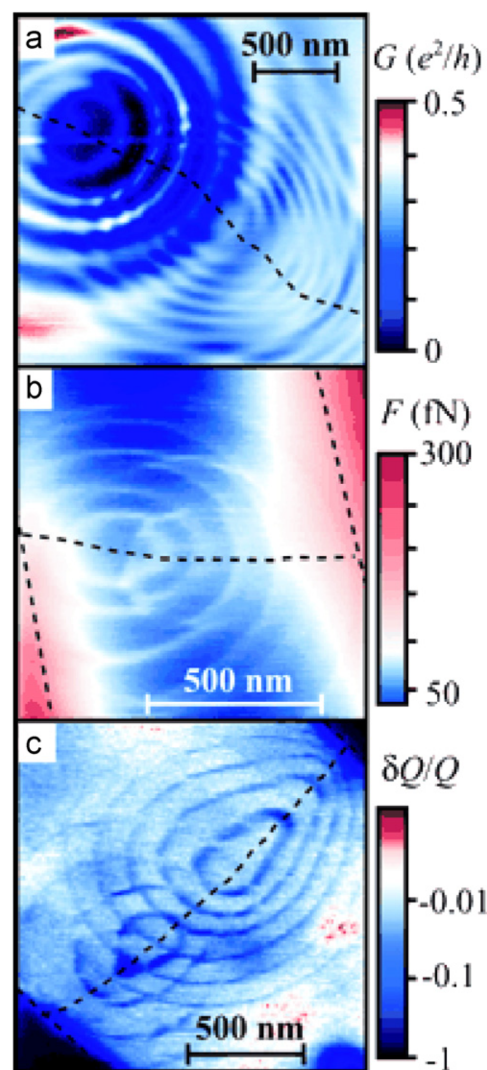

Fig. 1. Coulomb oscillations as a function of tip position. In all images, dashed lines show the location of the nanotube and contacts, determined from topographic AFM scans. (a) A single-electron scanning gate microscope (SGM) image of the conductance reveals two sets of concentric rings of conductance peaks from Coulomb oscillations on two dots in series in this nanotube. $T\sim6$ K, $V_{tip}=-200$ mV. (b) An e-EFM image of the force from a different device. An AC voltage at the resonant frequency of the cantilever is applied to the sample electrodes. Concentric rings of force peaks are seen, enclosing two dots in series. $T=0.6$ K, $V_{tip}=-400$ mV. (c) A single-electron EFM image of the Q degradation from a third device. Two sets of concentric rings where the Q is reduced enclose two dots in series. $T=0.6$ K, $V_{tip}=-300$ mV (adapted from Ref. [23]).

Directly imaging the surface potential variations at the nanoscale using EFM in thin films [24–26], or around domain boundaries [27] or structural defects in devices [6] shed light on the nature of electron transport in these materials. For instance, a uniform voltage drop found along multiwalled carbon nanotubes in the channel regime of field-effect transistors (FET) indicates that these nanotubes are diffusive conductor with finite resistance. In comparison, potential along metallic single-walled carbon nanotubes was nearly unchanged, suggesting the ballistic transport characteristic of such materials [6]. The quality and energy-level alignment at the nanotube-electrode contacts in these prototype nanoelectronics could be further investigated using scanning gate microscope and EFM [28]. Local potential variations observed in EFM studies revealed that strong dipole associated with O_2 adsorption on electrode modified the Schottky barriers at the contact, which is responsible for the n-type, p-type and ambipolar behavior observed in nanotubes-FET devices [28].

For nanomaterials, the procedure of attaching electrodes on individual nanoscaled entities in transport measurements is always a challenge. In these cases, EFM could be used in contactless measurement for electrical characterization and contributes unique information. A recent study on SWCNTs by high-resolution phase spectroscopy demonstrated that EFM is sensitive enough to detect the local electronic structures associated with van Hove singularities of SWCNTs adsorbed on silicon oxide surface [29]. Individual metallic and semiconducting SWCNTs could be distinguished without using attached electrodes.

DNA is another interesting molecular wire system, whose conductivity is under active debate due to the conflicting results obtained in electrical transport measurements [30]. Dirty contacts might be a contributing factor to the observed experimental inconsistency, along with other possibilities such as ionic conduction in ligand water adhesive to DNA molecules. To circumvent the complexities, several experimental schemes employing EFM have been implemented. In two independent experiments [31,32], DNA and CNTs coadsorbed on insulator

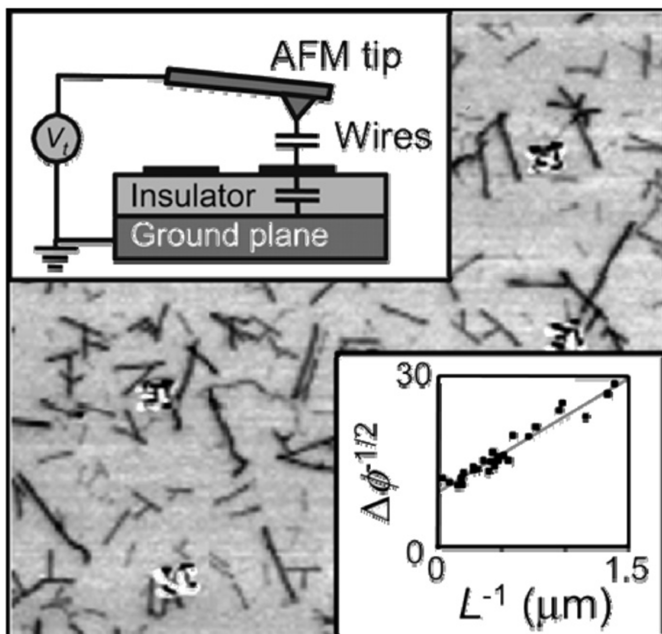

Fig. 2. Upper inset: experimental setup. An AFM cantilever is driven near its resonant frequency. The tip is scanned over a grounded oxidized Si wafer with the samples under study on its surface. After acquiring topography for each line, the tip is retracted by ~30 nm and the line retraced to obtain the electrostatic force data. A scanned conductance image is obtained by producing a gray scale plot of the phase lag Φ between the cantilever drive and oscillation as a function of tip position. Main panel: scanned conductance image for single-wall carbon nanotubes. Dark lines indicate shifts in Φ relative to the background value Φ_0 occurring whenever the tip is over a tube. The ~1 μm square features are evaporated Au alignment marks. Lower inset: plot of $(\Delta\Phi)^{-1/2} = (\Phi - \Phi_0)^{-1/2}$ versus the inverse tube length L^{-1} for 26 individual tubes. The data follow a straight line (adapted from Ref. [32]).

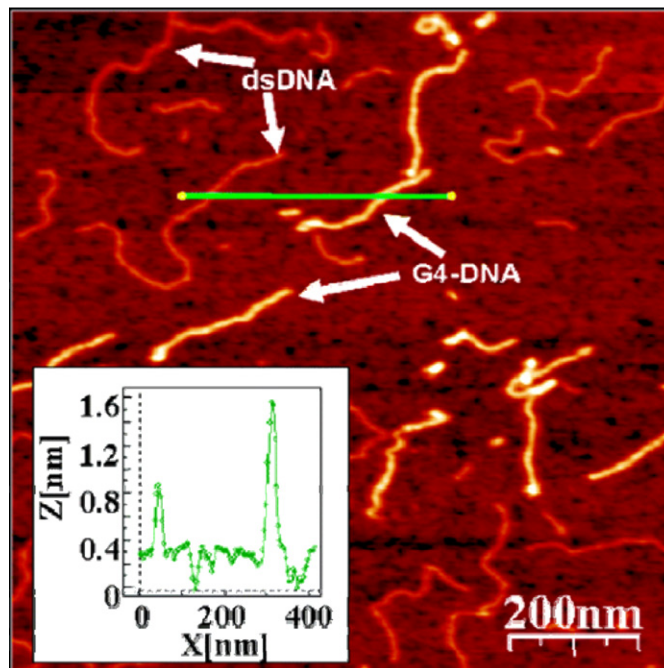

Fig. 3. AFM topography image of coadsorbed G4-DNA and dsDNA. A batch of G4-DNA molecules made of ~3200 base poly-(G) strands was imaged here. The inset shows a height profile along the green segment (adapted from Ref. [34]).

surface were investigated using EFM phase detection (Fig. 2) [32]. The small magnitude of phase shift signal observed on DNA strands with respect to the insulating substrate is in sharp contrast to that of CNTs, indicating distinct polarization of the two materials. The DNA strands in these studies were concluded to be insulating. In comparison, carbon nanotubes showed good conductivity as expected, with discernable differences in EFM phase shifts between metallic and semiconducting species. In a later experiment, the electrical properties of DNA were examined by using a charge injection and detection method [33]. It was found that charge injected from an EFM tip into DNA molecules could be either localized at a single spot or delocalized over the whole DNA segments. Such intriguing behavior has been attributed to the conformational changes of DNA molecules due to different sample preparation methods, suggesting an intrinsic reason for the elusive results in DNA electrical measurements. This conclusion seems to be validated by another study on different types of DNA molecules [34]. EFM phase detection, as shown in Fig. 3, revealed that double-stranded DNA have negligible polarizations compared with that of quadruplex helical structured DNA (G4-DNA), suggesting that the conductivity of biomolecules is sensitively dependent on their internal molecular structures [34].

Other biological systems involved in EFM studied include viruses. Each type of viruses showed distinguishable and characteristic capacitances, which were attributed to variation in constituting proteins in the envelope and the capsids [35]. It is proposed that, based on the fingerprint feature in capacitance spectra, EFM method could be used to directly detect and identify viruses at the single viron level.

2. Detection mode

EFM measurements are performed by using the Lift-mode technique, where the probe scans over the sample at a lift-height ranging from a few tens of nm to hundreds of nm with respect to the topographic surface. In the measurements, an EFM probe scans twice on each scanline of the sample. During the first pass, the topographical profile of the sample is obtained via intermittently contacting the probe with the surface. The probe is then biased and raised to a set height. The second scan is performed while maintaining a constant separation between the tip and local surface topography (life-mode, Veeco Instruments Inc.), or at a constant height relative to the average surface topography (linear-mode, Veeco Instruments Inc.). This operation principle ensures that the force exerted on an EFM probe is dominated by the long-range electrostatic interactions. Contributions from van der Waals force and chemical interaction are minimized because both interactions decay quite exponentially when the tip is moved away from sample surface.

AC detection method has been often used to detect the small change in amplitude [36], phase [29], or frequency [9,10,37] of the oscillating cantilever in response to the force gradients of Coulomb interactions. A functional diagram of EFM instrumentation is shown in Fig. 4.

In phase detection mode, the cantilever of an EFM probe is normally driven to oscillate at or close to its natural resonant frequency ω_0. For a freely oscillating cantilever with a spring constant of k, effective mass of m, and quality factor of Q, its frequency response can be modeled as a damped harmonic oscillator with Lorentzian profile. The phase angle ϕ (in units of radians) of the cantilever oscillation relative to the drive signal ω_0 can be expressed as

$$\phi = \tan^{-1}\left(\frac{m\omega\omega_0}{Q(k - m\omega^2)}\right) \quad (1)$$

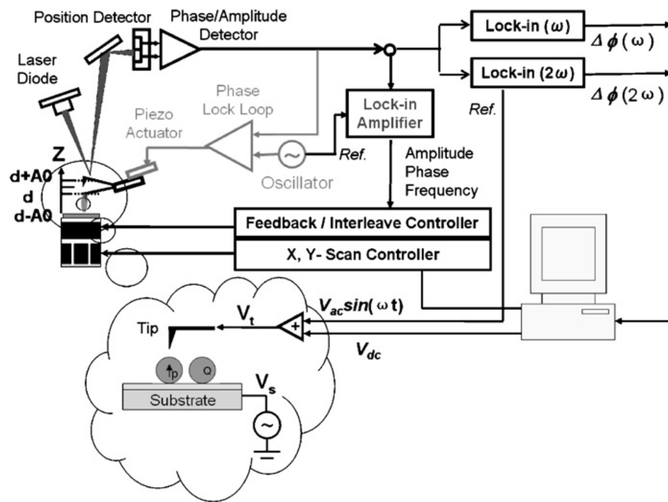

Fig. 4. An EFM experimental setup. Each line on sample surface are scanned twice: the first pass is a *tapping*-mode scan without applying voltage between the surface and the tip, yielding topographic information of the sample surface; on the second pass, an external bias was applied to the probe as it scans at a constant height above the surface while being dithered mechanically at its resonant frequency. The cantilever oscillation signal is fed into two lock-in amplifiers where the ω and 2ω components of the signal are isolated and fed back into the imaging software.

where ω is the actual vibrating frequency of the cantilever. For a freely oscillating cantilever, $\omega = \omega_0$, $\phi = \pi/2$, indicating a phase lag of $\pi/2$ between sinusoidal drive signal and cantilever oscillation.

As an EFM tip approaches the sample surface, the force gradient F' due to changes of tip–sample interactions modifies the effective spring constant k of the vibrating cantilever, thus affects its phase angle ϕ. Under the condition of $F' \ll k$ via limiting the cantilever oscillation to small amplitudes, the phase angle ϕ can be expressed by [39]

$$\phi = \tan^{-1}\left(\frac{k}{QF'}\right) \approx \frac{\pi}{2} - \frac{Q}{k}F' \tag{2}$$

Here $F' = \sum \partial F_i/\partial z$ represents the sum of the derivatives of all forces acting on cantilever in the surface normal direction z. If phase shift $\Delta\phi$ is defined as the phase delay away from the free oscillating state of cantilever, we then get

$$\Delta\phi \approx -\frac{Q}{k}F' \tag{3}$$

The equation suggests that the phase shift $\Delta\phi$ in EFM phase measurement is proportional to the overall force gradient between tip and sample. The sign of the phase angle shift is positive when the overall force acting on the tip is repulsive, and negative when the overall force is attractive.

In frequency detection (or frequency modulation) mode, instantaneous phase shift of the cantilever oscillation caused by changes in force gradient due to tip–sample interactions is used as an error signal in a feedback scheme; i.e., the frequency of the drive signal is modulated to maintain the cantilever oscillation at a constant phase relative to the drive signal [40]. The modulation of the drive frequency is recorded for information. Under the approximation of a harmonic oscillator, the new resonant frequency ω of cantilever can be written as [39]

$$\omega = \omega_0\left(1 - \frac{F'}{k}\right)^{1/2} \tag{4}$$

When the force gradients are small $F' \ll k$, ω can be approximated by the first two terms of the Taylor expansion. The frequency shift of the cantilever is then given by

$$\Delta\omega = |\omega - \omega_0| \approx \frac{\omega_0}{2k}F' \tag{5}$$

Apparently, the frequency shift $\Delta\omega$ in the measurements is also proportional to the overall force gradient F' of the tip–sample interactions.

The preferred methods of EFM are phase detection and frequency modulation, because the phase and frequency response of cantilever is faster than its amplitude response to the changes of tip–sample interactions and less susceptible to height variations on the sample surface. In particular, amplitude detection mode is not recommended for EFM used in vacuum because the maximum bandwidth of measurement is restricted by the time constant ($\sim 2Q/f_0$) of cantilever required for adjusting oscillation amplitude. When there is no dampening by the air or fluid around the cantilever, the Q factor becomes significantly larger ($\sim$up to 50,000) than that ($\sim$a few hundreds) in air, making amplitude response rather slow. A non-traditional amplitude-modulation inversion technique was introduced to overcome these drawbacks [38].

3. Analytical models for the tip–sample interaction

In contrast to AFM, where the tip–sample interaction is usually dominated by the van der Waals forces acting on the tip apex of a probe, an EFM probe experiences various electrostatic interactions that have a long-range character and larger magnitude than van der Waals forces. Because the commercial EFM probes have an integrated structure including the tip apex, cone and cantilever [41], a rigorous analysis of the tip–sample interactions must take into account every components of the probe influenced by different contributing interactions due to the nature of forces between tip and sample surface.

Extensive effort has been put forth to model the complex tip–surface interactions. Besides the approaches based on isolated point charges [13], uniform line charge [42], and parallel plate geometry [43,44] proposed in the early stage, analytical models based on perturbation theory and numerical simulations have also been reported [45,46].

Recently developed theoretical models have been more focused on the different tip shapes and both metallic and dielectric samples. Using generalized image charge method (GICM), electrostatic force may be calculated by simulating the tip as a distribution of point charges, whose position are obtained by fitting the tip shape to an equipotential surface; the sample is replaced by a series of image charges generated by tip charge [47]. An effective radius of the tip could then be derived from the force versus distance measurements on conductive substrates [48]. In contrast to metallic samples, where the force law mainly depends on the tip radius, the electrostatic interaction for an EFM tip on a dielectric sample was found to rely on the overall geometry of the probe [49].

The electric field distribution in a dielectric layer (polymer) sandwiched between tip–substrate gap was simulated by image charge method [50]. When tip–polymer distance is smaller than the thickness of polymer film, the simulation showed that the electric field generated by a negative tip bias of several volts could exceed the breakdown threshold of polymer.

The electrostatic forces acting on two types of commercial EFM probes were thoroughly analyzed using numerical simulation [51]. To simplify the calculation, the probes were approximated as a plate attached by a truncated cone ending with a hemisphere as shown in Fig. 5. The simulation results showed that the tip–sample interaction could be characterized by three distinct

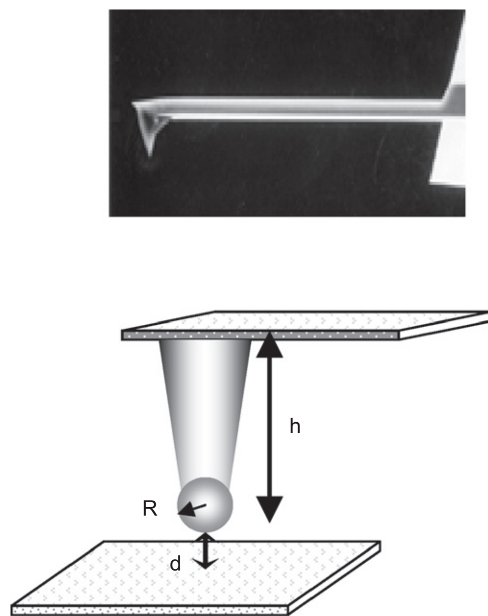

Fig. 5. (a) SEM photograph of an EFM probe from Veeco Instruments Inc. and (b) probe geometry used to model the tip–surface capacitance.

zones with different distance dependencies. For small distance d that is comparable to the size of tip apex R (~a few tens of nm), the simulation got a force law of $F' \propto 1/d^2$, which is consistent with the sphere–plane model that treats the charge on the tip as a point charge on tip apex [13]. For an intermediate distance when $R<d<h$, h (in the range of ~4 to ~10 μm) is the height of the pyramidal tip of an EFM probe, the dependence is approximately $F' \propto 1/d$, and agrees well with the uniformly charged line model [42]. When $d>h$, i.e. the tip is far from the sample surface, the force law is $F' \propto 1/d^3$. The above-mentioned three ranges correspond to the situations where the force is mainly localized on the tip apex, on the conical part of the probe, and on the probe as a whole, respectively. In typical EFM experiments, the tip–sample distance d is normally less than 1 μm, which is much smaller than the cantilever-to-sample distance h (~10 μm). So the total force gradient F' mainly comes from the tip apex and pyramid of the probe in such situations.

It is interesting to note that the different force dependences at varying tip–surface distance found in above-mentioned numerical method could be well reproduced by an analytical expression [52]. The model is derived from a superposition of infinitesimal surfaces of a capacitor system with the axial symmetry. The three force laws obtained in the previous numerical derivation appear to be the approximation result of a general formula of total force under different conditions.

A more general analytical model was developed recently to quantify charge measurement on EFM tip–sample systems with arbitrary geometries [18]. The essential feature of the method is to use the capacitive force gradient Δf_ε as a calibration for charge signal, and compare the charge frequency shift Δf_Q to the capacitive signal Δf_ε by computing the ratio $R = \Delta f_\varepsilon/\Delta f_Q$. This general formula holds for tip and sample with various shapes, and is also applicable when a sinusoidal voltage applied to EFM tip. After determining the tip–substrate capacitance through capacitive signal, the additional charge stored in nanostructure could be quantitatively calculated by the method.

For commercially available EFM probes, the tip apex radius is usually specified in the range of a few tens of nm [41]. Such variation in microscopic shape is found to be largely responsible for the discrepancy in force measurements using different EFM probes. One approach to circumventing this complexity is to use single-wall carbon nanotubes as probe. The uniform line charge model applicable to the high aspect ratio tip structure might help to improve the quantification accuracy [53]. In other situations, the capacitance between the tip and sample has been recognized as an effective venue to characterize the microscopic geometry of tip apex, and more importantly, the electric interaction between the tip and sample.

4. The characteristic capacitance of an EFM probe

The total electrostatic interactions acting on an EFM probe with respect to a conductive substrate can be viewed as a superposition of two component forces: capacitive interaction due to the tip–surface capacitor, and Coulombic forces due to the static charges and multipoles on substrate surface [13]. A generalized expression is given by [9,10]

$$F = \frac{1}{2}\frac{\mathrm{d}C_{\mathrm{s-t}}}{\mathrm{d}z}V_{\mathrm{t}}^2 + E_{\mathrm{s}}Q_{\mathrm{t}} \tag{6}$$

Here, the first term is associated with the charging energy of an empty capacitor formed between the tip and the substrate surface. $\mathrm{d}C_{\mathrm{s-t}}/\mathrm{d}z$ is the derivative of the tip–surface capacitance with respect to the tip-to-surface distance z. V_{t} is the voltage applied to tip with respected to the ground. $E_{\mathrm{s}}Q_{\mathrm{t}}$ is the Coulombic term. E_{s} represents the electric field at tip location only due to the static charges and/or multipoles on substrate surface. Q_{t} is the effective charge on the tip, including the charge generated on the tip due to tip bias V_{t}, plus the image charge induced by the static charge in the substrate.

When an AC voltage $V_{\mathrm{t}} = V_{\mathrm{dc}}+V_{\mathrm{ac}}\sin(\omega)$ is applied to the tip, the potential difference between the probe and substrate is then written as $V_{\mathrm{tot}} = \varphi+V_{\mathrm{dc}}+V_{\mathrm{ac}}\sin(\omega t)$, where φ is their contact potential difference. The modulated electric field generates an oscillating polarization in the sample on substrate surface and adds a component $f\{\varepsilon, g\}V_{\mathrm{ac}}\sin(\omega t)$ to E_{s}, where f is determined by sample dielectric constant ε and geometric parameters g of the tip–substrate junction. The amplitudes of the force components at ω and 2ω can be written as

$$F(\omega) = \left((V_{\mathrm{dc}} + \varphi)\frac{\mathrm{d}C_{\mathrm{s-t}}}{\mathrm{d}z} + E_{\mathrm{s}}C_{\mathrm{s-t}} + f(\varepsilon, g)(Q_{\mathrm{im}} + C_{\mathrm{s-t}}(V_{\mathrm{dc}} + \varphi))\right)V_{\mathrm{ac}} \tag{7}$$

$$F(2\omega) = \left(\frac{1}{2}f(\varepsilon, g)C_{\mathrm{s-t}} + \frac{1}{4}\frac{\mathrm{d}C_{\mathrm{s-t}}}{\mathrm{d}z}\right)V_{\mathrm{ac}}^2 \tag{8}$$

The force at 2ω is a function of the tip characteristic capacitance and sample polarizability, whereas the force component at ω depends on both instrument and sample factors such as tip voltage, local work function φ, surface charges and dipoles. In the case when no sample is presented in the tip–substrate junction, Eqs. (7) and (8) could be further approximated as

$$F(\omega) = \frac{\mathrm{d}C_{\mathrm{s-t}}}{\mathrm{d}z}(V_{\mathrm{dc}} + \varphi)V_{\mathrm{ac}} \tag{9}$$

$$F(2\omega) = \frac{1}{4}\frac{\mathrm{d}C_{\mathrm{s-t}}}{\mathrm{d}z}V_{\mathrm{ac}}^2 \tag{10}$$

Eq. (10) suggests that the characteristic capacitance of a given tip on bare substrate could be experimentally determined by measuring the force signal of $F(2\omega)$. Combining Eq. (10) with Eq. (3) or Eq. (5), it is readily to derive the z dependence of $\mathrm{d}^2C_{\mathrm{s-t}}/\mathrm{d}z^2$ after a measurement of the EFM probe's phase or frequency shift at the 2ω channel as a function of tip–substrate distance z. Then, a modeled tip structure is introduced, usually composed of a

combined structure of plate, cone and hemisphere with unspecified parameters of dimension, in order to get the analytical expression of tip capacitance as a function of z. Numerical fitting is then conducted to compute the best fit model parameters for d^2C_{s-t}/dz^2 versus z curves. The characterized tip is then used to measure the samples on the same substrate [9,10].

We recently proposed an alternative method to directly determine dC_{s-t}/dz by measuring the slope of EFM phase shift versus tip voltage characteristics [54]. The approach is summarized as follows.

For a planar conductive substrate with uniform surface electrical properties, the electric field E_s experienced by EFM tip due to the surface charges is expected to be constant for small tip–substrate separation, and so does the image charge Q_{im} on the tip. The derivative of Eq. (6) can be approximated by

$$F' \approx \frac{1}{2}\frac{d^2C_{s-t}}{dz^2}V_t^2 + \frac{dC_{s-t}}{dz}E_sV_t. \tag{11}$$

When a DC voltage of V_s is applied to the substrate, additional charges built up on the surface might account for the main contribution to the total electric field E_s. We assume the average electric field experienced by the tip were written as $E_s = g(s)V_s$, where $g(s)$ is a factor related to the tip geometry. At the condition when $V_s \gg V_t$, the first term in Eq. (11) is comparably smaller than the second term. Consequently, Eq. (11) could be further approximated as

$$F' \approx \frac{dC_{s-t}}{dz}g(s)V_sV_t = K_0V_t. \tag{12}$$

where $K_0 = (dC_{s-t}/dz)g(s)V_s$.

Eq. (12) suggests that by applying a sufficiently high voltage to the substrate, the tip–substrate interactions would be dominated by Coulombic interaction due to the charges stored on substrate surface, while the contribution from capacitive interaction remains unchanged. By this means, the derivative of the tip–sample characteristic capacitance dC_{s-t}/dz could be directly obtained by measuring the slope K_0 of phase shift ($\Delta\theta$) versus tip voltage (V_t) characteristics [54]. Compared to the aforementioned method of curve fitting to d^2C_{s-t}/dz^2, our scheme is a convenient approach to characterize EFM tip geometry.

5. Quantitative techniques and applications

Eqs. (9) and (10) suggest an effective approach to quantify static-charge and dielectric properties of materials using EFM, as long as the microscopic structure of probe used in the experiments is determined. In the simplest model, the electrostatic force between an EFM tip and a planar sample, which is viewed as a conducting sphere against a semi-infinite substrate of dielectric constant ε, can be calculated analytically by using the standard image charge technique.

Quantitative analysis of charge and dielectric properties has been performed on a few chemically synthesized nanocrystals including CdSe nanocrystals [9] and nanorods [55], PbSe nanocrystals [56], and self-assembled SiGe nanostructures [57]. After characterizing the capacitance (typically varies by a factor of 2–3 among different tips) of tip used in the measurements, the static dielectric constant of individual CdSe nanoparticles with ~5 nm

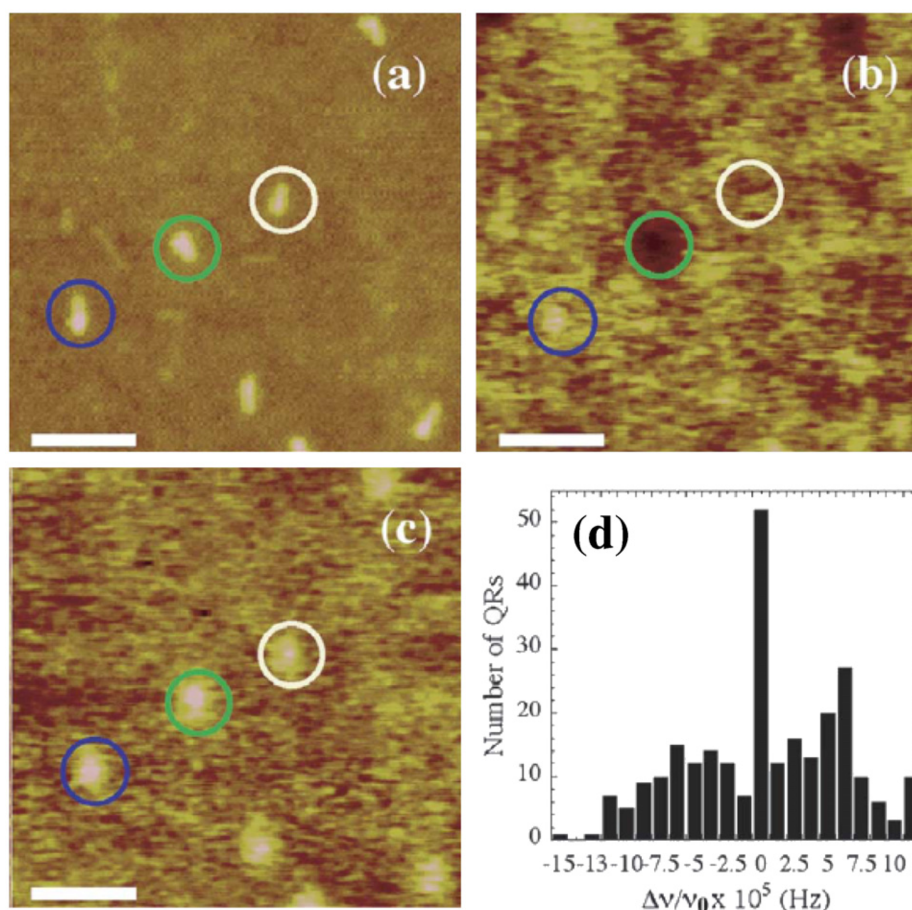

Fig. 6. EFM image of 50 nm long CdSe QRs with a 1:10 aspect ratio. (a) Height image. The QR width appears artificially enlarged due to the finite radius of the tip. Scale bar = 100 nm. (b and c) Cantilever frequency shifts recorded at $\omega[\Delta\nu(\omega)]$ and $2\omega[\Delta\nu(\omega)]$, respectively, with $V_{dc} = -\varphi$. The circled QRs (from left to right) correspond to negative, positive, and neutral QRs. Scale bar = 100 nm. (d) Histogram of QR relative frequency shift $\Delta\omega/\nu_0$ (adapted from Ref. [55]).

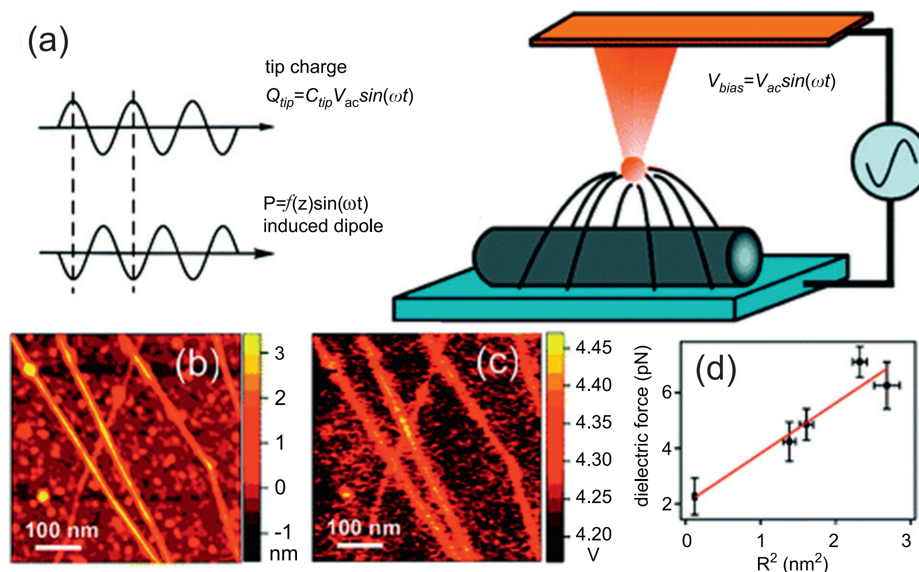

Fig. 7. (a) Schematic illustration of the scanning force microscopy approach to the near-DC polarization of individual carbon nanotubes. (b) Topography and (c) dielectric images from a typical scan. (d) Quadratic dependence of the dielectric response on nanotube radius (adapted from Ref. [58]).

diameter and capped by TOPO was determined to be ~8. The magnitude of the charge per nanocrystal is obtained by fitting Eq. (9) as a function of V_{dc}. The charge on CdSe nanoparticles in dark was found to be null within a measurement accuracy of ~0.1e and became more positive upon photoionization [9]. The situation differs in the case of CdSe nanorods (QR), which carry polarization surface charges typically ranging between −5e and 7e per QR, as shown in Fig. 6 [55]. The charge arises because the direction of the internal polarization of the quantum rod is not completely orthogonal to the surface normal along its entire length. The average line charge density was calculated to be ~0.028 e/nm on the CdSe QR. By using similar tip geometry approximation, the dielectric constant of PbSe nanocrystals with 12 nm diameter was estimated at >100, in comparison with the value of 250 for bulk PbSe [56]. It was found that the buried charges in the supporting surface formed by silicon oxide thin films on top of doped silicon substrate could also induce appreciable polarization of the nanocrystals. For SiGe quantum dots grown on silicon on insulator, the dielectric constant was estimated to be 12 when taking into considering of the sample geometry in dielectric calculations [57].

Determine the dielectric response of carbon nanotubes is of importance for potential applications of this unique material as nanoelectronic components. Nevertheless, conventional ensemble measurements are always overwhelmed by the coexistence of nanotubes with different diameters and chiralities in the as-produced samples. Chen et al. recently reported an EFM scheme to quantitatively characterize the low-frequency dielectric polarization of individual single-walled carbon nanotubes (SWCNT) deposited on Si substrate with thin oxide layer (Fig. 7) [58]. The authors measured $F(2\omega)$ signal of single nanotubes as a function of the tube diameters. Using a solid dielectric cylinder model for nanotubes and a simulated tip structure derived from the experimentally measured tip characteristic capacitance, the near static dielectric constant in the transverse direction of nanotube is calculated to be ~10 for both metallic and semiconducting nanotubes. The longitudinal polarizability is determined to be about 100 times larger than that in transverse direction, indicating the highly anisotropic electronic structure in this unique 1D material.

It should be noted that the effect of water molecules adsorbed on sample surfaces has not been taken into consideration in the above discussion on dielectric measurements. In fact, water molecules are presented on both sample surface and tip apex in all experiments conducted under ambient conditions. Even in dry nitrogen atmosphere, this contamination layer is hardly completely removed unless appropriate measures are taken. Nevertheless, it is amazing that most material surfaces seem to be insensitive to the humidity environments and could still generate marked image contrasts in routine EFM experiments. Previous studies of water thin films seemed to indicate that the effect of water molecules on surface polarizability becomes more significant when mobile ions present on sample surfaces [59]. Given the fact that the dielectric constant of water in bulk phase at ambient condition is exceptionally large (~78), extra attentions should be taken in quantitative studies of electric properties using EFM.

Perspectives: The combined capabilities of imaging surface morphology and probing local electrical properties demonstrated by EFM and related techniques allow facile characterization of structures and materials at the nanoscale. The knowledge gained in these studies directly benefits many applied research projects and also provides an insightful view of the novel behaviors governed by quantum effects. The broad range of applications of EFM will be substantially strengthened by advances in reliable quantification method, which would have significant impacts on physics, material science, chemistry and biological systems.

Acknowledgments

This work is supported by the National Basic Research Program of China (2007CB936800) and Chinese Academy of Sciences (KJCX2-YW-M04). Financial support from National Science Foundation of China (90406019) is also gratefully acknowledged.

References

[1] A.D. Yoffe, Adv. Phys. 50 (2001) 1.
[2] E.A. Boer, M.L. Brongersma, H.A. Atwater, R.C. Flagan, L.D. Bell, Appl. Phys. Lett. 79 (2001) 791.
[3] E. Bussmann, D. Kim, C. Williams, Appl. Phys. Lett. 85 (2004) 2538.
[4] Y. Katano, T. Doi, H. Ohno, K. Yoh, Appl. Surf. Sci. 188 (2002) 399.
[5] S. Saraf, Y. Rosenwaks, Surf. Sci. 574 (2005) L35.
[6] A. Bachtold, M.S. Fuhrer, S. Plyasunov, M. Forero, E.H. Anderson, A. Zettl, P.L. McEuen, Phys. Rev. Lett. 84 (2000) 6082.
[7] X. Zhou, S.A. Dayeh, D. Wang, E.T. Yu, Appl. Phys. Lett. 90 (2007) 233118.

[8] J.E. Spanier, A.M. Kolpak, J.J. Urban, I. Grinberg, et al., Nano. Lett. 6 (2006) 735.
[9] T. Krauss, L. Brus, Phys. Rev. Lett. 83 (1999) 4840.
[10] O. Cherniavskaya, L.W. Chen, M.A. Islam, L. Brus, Nano. Lett. 3 (2003) 497.
[11] Y. Martin, D.W. Abraham, H.K. Wickramasinghe, Appl. Phys. Lett. 52 (1987) 1103.
[12] J. Matey, J. Blanc, J. Appl. Phys. 57 (1985) 1437.
[13] B.D. Terris, J.E. Stern, D. Rugar, H.J. Mamin, Phys. Rev. Lett. 63 (1989) 2669.
[14] K. Domanský, Y. Leng, C.C. Williams, J. Janata, D. Petelenz, Appl. Phys. Lett. 63 (1993) 1513.
[15] T. Mélin, D. Deresmes, D. Stiévenard, Appl. Phys. Lett. 81 (2002) 5054.
[16] H. Diesinger, T. Mélin, D. Deresmes, D. Stiévenard, T. Baron, Appl. Phys. Lett. 85 (2004) 3546.
[17] T. Mélin, H. Diesinger, D. Deresmes, D. Stiévenard, Phys. Rew. Lett. 92 (2004) 166101.
[18] T. Mélin, H. Diesinger, D. Deresmes, D. Stiévenard, Phys. Rev. B 69 (2004) 035321.
[19] M. Zdrojeka, T. Mélin, H. Diesinger, D. Stiévenard, W. Gebicki, L. Adamowicz, J. App. Phys. 100 (2006) 114326.
[20] M. Zdrojeka, T. Mélin, H. Diesinger, D. Stiévenard, B. Jouault, M. Wozniak, A. Huczko, W. Gebicki, L. Adamowicz, App. Phys. Lett. 86 (2005) 213114.
[21] M. Paillet, P. Poncharal, A. Zahab, Phys. Rev. Lett. 94 (2005) 186801.
[22] R. Stomp, Y. Miyahara, S. Schaer, Q. Sun, H. Guo, P. Grutter, Phys. Rev. Lett. 94 (2005) 056802.
[23] M.T. Woodside, P.L. McEuen, Science 296 (2002) 1098.
[24] M. Drndić, R. Markov, M.V. Jarosz, M.G. Bawendi, M.A. Kastner, N. Markovic, M. Tinkham, Appl. Phys. Lett. 83 (2003) 4008.
[25] B.J. Rodriguez, W.C. Yang, R.J. Nemanich, Appl. Phys. Lett. 86 (2005) 112.
[26] L.W. Chen, O. Cherniavskaya, A. Shalek, L.E. Brus, Nano. Lett. 5 (2005) 2241.
[27] Z.H. Hu, M.D. Fischbein, M. Drndić, Nano. Lett. 5 (2005) 1463.
[28] X. Cui, M. Freitag, R. Martel, L. Brus, Ph. Avouris, Nano. Lett. 3 (2003) 783.
[29] J.S. Heo, M. Bockrath, Nano. Lett. 5 (2005) 853.
[30] D. Porath, A. Bezryadin, S. de Vries, C. Dekker, Nature 403 (2000) 635.
[31] C. Gómez-Navarro, F. Moreno-Herrero, P.J. de Pablo, J. Colchero, J. Gómez-Herrero, A.M. Baró, Proc. Natl. Acad. Sci. 99 (2002) 8484.
[32] M. Bockrath, N. Markovic, A. Shepard, M. Tinkham, L. Gurevich, L.P. Kouwenhoven, M.W. Wu, L.L. Sohn, Nano. Lett. 2 (2002) 187.
[33] T. Heim, T. Mélin, D. Deresmes, D. Vuillaume, Appl. Phys. Lett. 85 (2004) 2637.
[34] H. Cohen, T. Sapir, N. Borovok, T. Molotsky, R.D. Felice, A.B. Kotlyar, D. Porath, Nano. Lett. 7 (2007) 981.
[35] R.I. MacCuspie, N. Nuraje, S.Y. Lee, A. Runge, H. Matsui, J. Am. Chem. Soc. 130 (2007) 887.
[36] M.J. Gordon, T. Baron, Phys. Rev. B 72 (2005) 165420.
[37] O. Cherniavskaya, L.W. Chen, V. Weng, L. Yuditsky, L.E. Brus, J. Phys. Chem. B 107 (2003) 1525.
[38] S.N. Magonov, V. Elings, M.H. Whangbo, Surf. Sci. 375 (1997) L385.
[39] R. García, R. Pérez, Surf. Sci. Rep. 47 (2002) 197.
[40] See 〈http://www.veeco.com/pdfs.php/260〉.
[41] For example, MESP-ESP Series Probes from Veeco Instruments.
[42] H.W. Hao, A.M. Baro, J.J. Saenz, J. Vac. Sci. Technol. B 9 (1991) 1323.
[43] D. Schaadt, E. Yu, S. Sankar, A. Berkowitz, Appl. Phys. Lett. 74 (1999) 472.
[44] R. Dianoux, F. Martins, F. Marchi, C. Alandi, F. Comin, J. Chevrier, Phys. Rev. B 68 (2003) 045403.
[45] S. Gäomez-Moñivas, J.J. Sáenz, Appl. Phys. Lett. 76 (2000) 2955.
[46] G.M. Sacha, J.J. Sáenz, Appl. Phys. Lett. 85 (2004) 2610.
[47] G.M. Sacha, C. Gómez-Navarro, J.J. Sáenz, J. Gómez-Herrero, Appl. Phys. Lett. 89 (2006) 173122.
[48] G.M. Sacha, A. Verdaguer, J. Martínez, J.J. Sáenz, D.F. Ogletree, M. Salmeron, Appl. Phys. Lett. 86 (2005) 123101.
[49] S. Gómez-Moñivas, L.S. Froufe-Pérez, A.J. Caamaño, J.J. Sáenz, Appl. Phys. Lett. 79 (2001) 4048.
[50] S.F. Lyuksyutov, P.B. Paramonov, R.A. Sharipov, G. Sigalov, Phys. Rev. B 70 (2004) 174110.
[51] S. Belaidi, P. Girard, G. Leveque, J. Appl. Phys. 81 (1997) 1023.
[52] S. Hudlet, M. Saint Jeana, C. Guthmann, J. Berger, Eur. Phys. J. B 2 (1998) 5.
[53] N.R. Wilson, J.V. Macpherson, J. Appl. Phys. 96 (2004) 3565.
[54] G.C. Qi, Y.L. Yang, X.H. Qiu, C. Wang, J. Appl. Phys. 103 (2008) 114311.
[55] R. Krishnan, M.A. Hahn, Z. Yu, J. Silcox, P.M. Fauchet, T. Krauss, Phys. Rev. Lett. 92 (2004) 216803.
[56] C.H. Ben-Porat, O. Cherniavskaya, L. Brus, K.S. Cho, C.B. Murray, J. Phys. Chem. A 108 (2004) 7814.
[57] E. Tevaarwerk, D.G. Keppel, P. Rugheimer, M.G. Lagally, M.A. Eriksson, Rev. Sci. Instrum. 76 (2005) 053707.
[58] W. Lu, D. Wang, L. Chen, Nano. Lett. 7 (2007) 2729.
[59] J. Hu, X.D. Xiao, M. Salmeron, Appl. Phys. Lett. 67 (1995) 476.